Full length article

MRI-guided liposomes for targeted tandem chemotherapy and therapeutic response prediction

Lili Ren [1], Shizhen Chen [1], Haidong Li, Zhiying Zhang, Jianping Zhong, Maili Liu, Xin Zhou *

Key Laboratory of Magnetic Resonance in Biological Systems, State Key Laboratory of Magnetic Resonance and Atomic and Molecular Physics, National Center for Magnetic Resonance in Wuhan, Wuhan Institute of Physics and Mathematics, Chinese Academy of Sciences, Wuhan 430071, China

ABSTRACT

Liposomes are effective drug delivery systems that can be functionalized with imaging contrast agents, providing both diagnosis and monitoring of disease treatment. Here we describe the design of a theranostic liposomal drug delivery system whose biodistribution can be real time imaged by contrast enhanced MRI and can achieve tandem chemotherapy drug delivery. Because T_1 relaxation of MRI depends upon the chemical structure of contrast agent as well as its interaction with neighbor environment, we rationally designed a functional liposome for *in vivo* T_1 enhanced MRI. The liposome shows a 36-fold higher T_1 relaxation rate over the commercial MRI contrast agent Omniscan® and a long circulation time up to 300 min *in vivo*. Moreover, the multifunctional liposome carries both hydrophobic and hydrophilic chemotherapeutic drugs, can synergistically enhance therapeutic effects of multiple drugs and selectively deliver them to lung tumors, leading to lower doses, toxicity and sustained release. The nanoparticles, which exhibit favorable biodistributions to tumors, offer new possibilities for the simultaneous delivery of more than one drug and the evaluation of therapeutic response *in vivo* by T_1 enhanced MRI.

Statement of Significance

Cancer cells invoke different mechanisms to resist cancer therapies, particularly when delivering a single agent in a given therapy. The combination of two (or more) thermotherapy agents provides a promising way to circumvent such situations of drug resistance, due to a favorable synergistic effect that "tricks" the drug resistance mechanism.
However, challenges to the simultaneous delivery of two drugs prevail, especially with regards to the simultaneous delivery of hydrophobic and hydrophobic drugs. Furthermore, non-invasive in vivo imaging of drug distribution enables the real-time monitoring and prediction of therapeutic responses to treatment.
In this study, we rationally designed a theranostic liposomal drug delivery system whose biodistribution can be imaged via T_1-weighted MRI in real-time and can achieve tandem chemotherapy drug delivery. This original study will be of considerable use to the wider drug delivery community.

© 2016 Acta Materialia Inc. Published by Elsevier Ltd. All rights reserved.

1. Introduction

Lung cancer is the leading cause of cancer death worldwide [1–4]. Non-small-cell lung cancer (NSCLC) accounts for over 80% of all lung cancer death cases. Despite the introduction of promising new chemotherapeutic agents for lung cancer, the average patient five-year survival rate remains low (5−15%) and this rate has persisted for decades [2,5,6]. These discouraging statistics are due, in part, to the lack of suitable drug delivery systems. Conventional drug delivery approaches neither deliver nor maintain sufficiently high drug concentrations at the site of solid lung tumors, leading to a lack of efficacy at treating the tumor, as well as adverse effects to the surrounding healthy tissues. Recent advances in chemotherapy and targeted therapy provide new treatment options for this disease. Indeed, current research efforts at treating NSCLC have focused on the precise intracellular delivery of drugs and diagnostic agents to selected target cell populations [7–10].

On the other hand, cancer cells invoke different mechanisms to resist cancer therapies, particularly in single agent administration.

This seriously weakens the efficacy of anticancer drugs. Combination regimens may change this awkward situation. Paclitaxel (PTX) and carboplatin (CBP) are two established anticancer drugs [1,3–5,11–13]. When used together, they have been shown to result in a more effective strategy for treating advanced NSCLC. Although this doublet chemotherapy looks promising for NSCLC, there are still serious side effects, including nephrotoxicity, myelotoxicity, neurotoxicity, vomiting and nausea [3,14]. Drugs loaded in one particle with controlled manner may overcome these obstacles. The concept of dual drug-loaded liposome was investigated by little researches. A phase I study of a novel liposome with cytarabine and daunorubicin for patients with refractory acute leukemia was conducted and followed by a subsequent phase II trial. The phase III trial is currently underway [15]. Additional dual drug-loaded liposomes, irinotecan/floxuridine and irinotecan/cisplatin, were successfully developed to treat colorectal cancer and small cell lung cancer, respectively [16,17]. These drugs are all hydrophilic. Based on our former studies of PTX-loaded liposomal system, here we look forward to design a more compatible PTX-CBP-loaded liposome [18].

To minimize side effects or damage to healthy tissue while achieving an effective therapy, liposomes, which have a hydrophilic core and a hydrophobic bilayer, are promising carriers for delivery of PTX, DDP (cisplatin, an analogue of CBP) and CBP [7,19–26]. The preparation of PTX, solubilized in a mixture of Cremophor EL (polyethoxylated castor oil) and ethanol to overcome its poor solubility in water, can give rise to undesirable effects [19–22]. It is already known that the liposomal PTX can overcome this obstacle and is beneficial to the phase II study of NSCLC patients with malignant pleural effusions [27]. Furthermore, liposomal drug delivery can be targeted to tissues in a selective manner, reducing the dose required and the off-target toxicity [24]. The folate receptor-targeted CBP liposome has been shown to improve the drug potency and reduce the toxicity in metastatic ovarian cancer [28]. A ligand-modified, PTX-loaded liposome could be targeted to mitochondria, enhancing anti-tumor efficacy and reducing non-specific toxicity [29].

Recently, research has focused on the development of nanoconstruct tools that incorporate multiple functionalities including capabilities for multimodal imaging to enable the simultaneous diagnosis and therapy. MRI-guided drug delivery combining cancer therapy and detection can help monitor the clinical response in real-time and could lead to personalized therapies [30,31]. Commonly used T_1 contrast agents, such as Gd chelates, can shorten the spin-lattice relaxation time of nearby protons and yield positive MRI contrast in T_1-weighted MRI images. The seven unpaired electrons of Gd (III) create a strong local magnetic field that fluctuates at the rate at which the complex tumbles in solution. In order to improve T_1 relaxation, we have rationally designed a functional liposome for optimization of the relaxation and circulation time. Additionally, Gd chelates are biodistributed non-specifically and rapidly eliminated from the body [30]. Liposomes that are loaded with suitable contrast agents can help overcome these obstacles, leading to an improved MRI readout [31–33].

In this article, a new and universal combination treatment drug delivery system was developed for targeting NSCLC (Fig. 1), including both hydrophilic (CBP) and hydrophobic (PTX) drugs. The targeted peptide c(RGDyK) tethered to the surface of the liposome, is recognized by $\alpha_v\beta_3$ integrin receptor, which is overexpressed in many tumor cells. Receptor-mediated liposome endocytosis and subsequent release of the contents could enhance the diagnostic and therapeutic results upon administration [7,8,34–36]. The cancer cells targeted with the multifunctional liposomes were readily detectable by MRI and confocal microscopy. Furthermore, the MRI-guided liposome showed great cancer-targeting efficiency and thus great potential to improve the lung cancer imaging and therapy and the outcomes of cancer patients.

2. Materials and methods

2.1. Liposome preparation

The peptide-lipid conjugates c(RGDyK)-PEG2000-DSPE were synthesized using cross-linker 1-(3-dimethylaminopropyl)-3-ethyl carbodiimide hydrochloride (EDC, Medpep, China) and N-hydroxysuccinimide (NHS, Sigma, USA) first [37,38]. COOH-PEG2000-DSPE (NANOCS, USA) was dissolved in PBS buffer. Then appropriate amounts of NHS and EDC were added. After incubation at room temperature for 30 min, c(RGDyK) (GL Bioche, China) was added, followed by 10 h incubation. Excess unreacted peptides were removed by dialysis (2000 D). The conjugated lipid was then lyophilized for the following procedures.

Dual drug-loaded liposome (RGD-CPGd-L) was prepared by the thin film hydration method, followed by membrane extrusion [7,17,37,39]. 15 mg of lipids, DSPC (Corden Pharma, Switzerland), DSPG (Corden Pharma, Switzerland), MPEG-2000-DSPE (Corden Pharma, Switzerland) and c(RGDyK)-PEG2000-DSPE at a molar ratio of 7:2:1:0.5, were mixed and dissolved in 1 mL chloroform/methanol/water (1:1:0.3, v/v/v). PTX (Shyuanye, China) was added to the lipid solution at a molar ratio of 1:30 (drug to lipid). The solution was dried in vacuum to form a film and placed under high vacuum overnight. The film was then hydrated with 100 mM Gd-DTPA-BMA (Chemlin, China) and 0.01 mM CBP (Adamas, China) to form multilamellar vesicles. These vesicles were sonicated in water bath for 10 min and subsequently extruded 10 times through a 0.2-μm pore size filters. The free PTX was excluded by centrifugation for 10 min at 2000 rpm. The exterior buffer of the liposome was exchanged by 1% glucose via dialysis (10 kD) for 4 h, followed by lyophilization for use [29,31,40].

Rhodamine-labeled liposome (Rh-L), composed of DSPC, DSPG, MPEG-2000-DSPE, c(RGDyK)-PEG2000-DSPE and Rhod-DMPE (Avanti, USA) at the molar ratio of 7:2:1:0.5:0.2, was prepared using a method similar to that described above. The whole process was protected from light [26,31,38,41].

The particle size and zeta potential of the liposome was determined by dynamic light scattering with a particle analyzer (ZS, Malvern, UK). Transmission electron microscopy was carried out with 1% phosphotungstic acid negative staining and visualized using a JEM2010 electron microscope (JEOL, Japan). The peptide-lipid conjugate c(RGDyK)-PEG2000-DSPE was verified by UV–vis spectrophotometer (Thermo, USA) and mass spectroscopy (Agilent, USA). The stability of RGD-CPGd-L in distilled water and fetal bovine serum (Boster, China) was also monitored by UV–vis spectrophotometer at room temperature.

2.2. Quantification of PTX, Gd-DTPA-BMA and CBP

The content of PTX incorporated in liposome was detected by HPLC (1200 Series, Agilent, USA). Specifically, the liposome was diluted by adding water and acetonitrile to 0.5 mL. PTX was extracted by adding 4.0 mL of tert-butyl methyl ether and mixing for 30 s. The mixture was centrifuged for 15 min at 300g, after which 3 mL of the organic layer was transferred and evaporated. The residue was dissolved with 100 μL of 7/3 acetonitrile/water mixture. 50 μL of the solution was injected into a C18 column guard. The flow rate was 1.0 mL/min. The detection wavelength was at 227 nm. The drug concentration was calculated from standard curves. This assay was linear over the concentration range from 1 μg to 500 μg [21,29].

The content of Gd-DTPA-BMA and CBP of the liposome were determined by amount of Gd and Pt detected by ICP-AES (IRIS Intrepid II XSP, Thermo, USA) respectively [42]. The sample was diluted with 0.5 mL water before adding 2 mL HNO_3 and heated
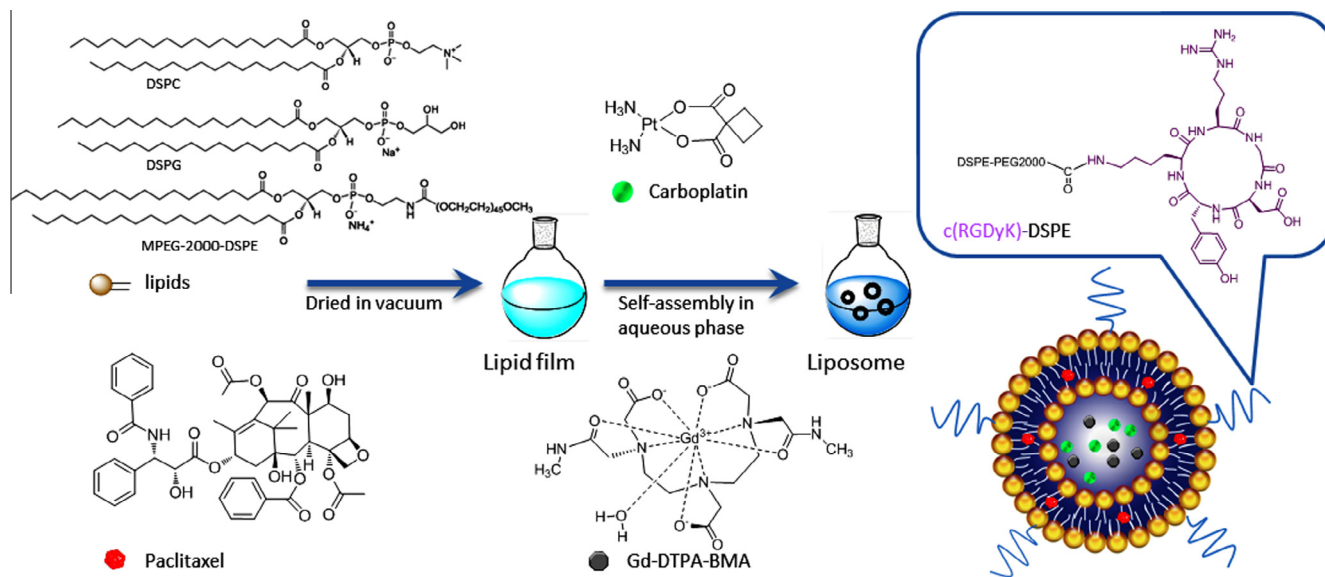
Fig. 1. Schematic diagram of PTX/CPB/Gd-DTPA-BMA-loaded and c(RGDyK)-modified liposome (RGD-CPGd-L), which can self-assemble in aqueous phase and target to tumor cell.

to approximately 150 °C for 30 min. Thereafter, the sample was diluted to 10 mL with water. Calibration was done with gadolinium and platinum ICP standard solution [43].

2.3. Characterization of contrast properties

The MR contrast effect of the liposome was examined by measuring the proton longitudinal relaxivity r_1, of which the definition is the slope of the concentration dependence given as $1/T_1 = 1/T_{10} + r_1[Gd]$, where T_1 is the longitudinal relaxation time, T_{10} is the longitudinal relaxation time in the absence of paramagnetic substances. The T_1 of liposome with different concentrations at 25 °C was measured by 500 MHz NMR spectrometer (Avance 500, Bruker, USA) using a standard inversion-recovery pulse sequence.

MR images were taken with a 7 T MRI scanner (BioSpec 70/20 USR, Bruker, USA) using 1% agarose phantom to mimic the MRI properties of biological tissue. Different concentrations of liposome were added into the phantom. T_1-weighted MR images were taken by standard multislice spin-echo pulse sequence with an echo time (TE) of 11 ms and a repetition time (TR) of 500 ms. The field of view was 6×6 cm^2, matrix size was 256×256 and slice thickness was 15 mm [44].

2.4. Cell culture and cancer model

The non-small-cell lung cancer cell A549, H1299 and human embryonic lung fibroblast WI-38 were purchased from the cell bank of Chinese academy of sciences (Shanghai, China). The tumor cells and normal cells were cultured in IMDM (Iscove's Modified Dulbecco's Medium, Boster, China) and MEM (minimum essential medium, Boster, China) respectively, supplemented with 10% fetal bovine serum (Boster, China), 100 U/mL penicillin (Boster, China) and 100 U/mL streptomycin (Boster, China) in a humidified air with 5% CO$_2$ at 37 °C.

BALB/c male nude mice (aged 5–6 weeks, approximately 20 g) were purchased from Human SJA Laboratory Animal Co., Ltd. All experimental protocols in this study were approved by Animal Care and Use Committees at the Wuhan Institute of Physics and Mathematics, the Chinese Academy of Sciences. The mice were

inoculated subcutaneously with A549 cells (1×10^6 cells of each) on the legs and used for MRI after 1 week breeding.

2.5. In vitro targeting effect

About 1×10^5 cells (A549, H1299 and WI-38, respectively) were seeded on cover slips placed in cell culture dishes. The regular culture mediums were removed when the cell confluence reached to 30–40%. Culture medium containing the rhodamine labeled liposome was added. After 4 h of incubation at 37 °C, cells were incubated with DAPI for 5 min for nuclear staining. All the cells were washed at least three times with PBS. The fluorescence images were taken by confocal laser scanning microscope (A1R/A1, Nikon, Japan) [7,29].

2.6. Cytotoxicity assay

About 1×10^4 cells (A549, H1299 and WI-38, respectively) were seeded per well in 96-well plates and cultured for 24 h. Different groups of liposomes were diluted with the medium and added to the well. After incubation for 48 h, cells were washed with PBS (pH 7.4) three times. MTT was added to the culture medium to the final concentration of 0.5 mg/mL during the last 4 h. 200 μL DMSO was added per well after removing the medium. The OD 490 nm for each well was measured by ELISA plate reader (Spectra MAX 190, Molecular Devices, USA) [7,34,45].

2.7. In vivo contrast properties

7 T MRI provided monitoring of liposome gathering in tumor-bearing mice by repeat scanning prior to treatment and post-treatment. A549 xenograft mice were oriented in prone position and the legs were fixed. The mice were initially anesthetized with 3% isoflurane, and then 1% isoflurane controlled by Matrx (USA). The respiratory cycle was monitored by a pneumatic pillow. T_1-weighted MRIs were obtained before and after tail intravenous administration of the dual drug-loaded liposome and Omniscan® (GE Healthcare, Ireland) using a spin-echo technique (TE = 11 ms, TR = 400 ms, 1-mm slice thickness, average = 4, matrix size = 256×256, FOV = 4×4 cm^2) [31,42]. The concentration of Gd was 0.1 mmol/kg both in the liposome and omniscan group.

T_1 was detected by a saturation-recovery technique (TR = 5000, 3000, 2000, 1200, 800, 500, 300, 200, 150, 120, 100 ms). Image reconstruction and analysis were performed by ParaVision 5.0. Increase of R_1 represents the extent of contrast enhancement at the function of contrast agent, which can be calculated as $(1/T_{1(t)} - 1/T_{1(0)})/1/T_{1(0)} \times 100\%$. $T_{1(t)}$ is the T_1 value at time point t after administration of the contrast agent. $T_{1(0)}$ is the T_1 value of the untreated tumor tissue [31].

2.8. Assessment of therapeutic effect by MRI

Therapeutic effect of dual drug-loaded liposome on tumor was evaluated by 7 T MRI scanner. A549 tumor bearing mice were used after 7 days post-tumor inoculation [31]. The fixation and anesthesia process were the same as above. RGD-CPGd-L was injected via tail vein at 500 mg/kg (about 53.10 mg/kg Gd-DTPA-BMA, 4.70 mg/kg PTX and 1.12 mg/kg CBP). The control group was injected with the same volume saline as the medicated group. When testing the tumor volume of control group, the same amount of RGD-Gd-L (about 53.10 mg/kg Gd-DTPA-BMA) was used. T_1-weighted MRIs were obtained 1 h after administration of the contrast agent-loaded liposome. The drugs were injected on days 0, 2, 4, 7, 10, 14 and 16. The MRIs were taken on day 0, 10, 16 and 23 with the same parameters as 2.7. Image analysis was performed by ParaVision 5.0. Regions of interest were identified using a mouse atlas of anatomy. The tumor volume was estimated as the sum of the tumor volumes of all slices. The mice weight was monitored all through the experiment, evaluating the systemic toxicity of the liposome [29,42].

To further study the toxicity of the liposome on main organs of the mice, kidney, spleen and liver were dissected from the mice for histological analysis carried out after the last examination by MRI. The samples were fixed in 4% paraformaldehyde and paraffin embedded for hematoxylin and eosin (H&E) staining. The samples were sectioned at 10-μm thickness and observed by Nikon microscope (Japan) [10,41,42,44].

2.9. Statistical analysis

Quantitative data are presented as mean ± standard deviation (SD). All data analysis and plotting were performed with OriginPro 8.0 data analysis software (OriginLab Corporation, Northampton, MA).

3. Results and discussion

3.1. Characterizations of liposome

The dual drug-loaded targeted liposome RGD-CPGd-L with contrast agent and gadodiamide, was prepared by a film hydration method followed by extrusion [7,17,37,39]. The structure of the liposome is showed in Fig. 1. The hydrophobic anticancer drug PTX can be located in the lipid double layer. The hydrophilic anticancer drug CBP and contrast agent Gd-DTPA-BMA are located in the cores of the liposome. Further peptide modifications can realize active delivery of drugs and contrast agents to the tumor. The peptide-lipid conjugate c(RGDyK)-PEG2000-DSPE has an absorbance around 270 nm similar to c(RGDyK) (Fig. 2a), indicating the successful conjugation of COOH-PEG2000-DSPE and c(RGDyK). The mass spectrometry further confirmed the conjugate of the lipid and RGD peptide (Fig. S1). The spherical particles can be seen by TEM with diameters around 128 nm (Fig. 2b). The relaxivity of the targeted drug-loaded liposome RGD-CPGd-L was 4.24 mM^{-1} s^{-1} per Gd atom (Fig. 2c). To verify the positive T_1 contrast properties, agarose phantoms were used to stimulate tumor tissue. As

seen in the T_1-weighted images of the phantoms with 0, 0.05 and 0.50 mM Gd-DTPA-BMA-loaded liposome (Fig. 2c), the MRI signal of sample 3 was much higher than that of pure agarose (sample 1), demonstrating the enhanced T_1 MR contrast property. RGD-CPGd-L displayed good physical stability over 24 h when reconstituted either in water or serum (Fig. 2d), which was beneficial for following experiments. As shown in Table 1, contrast agent and two anticancer drugs with different properties and mechanisms of drug action were successfully encapsulated in the liposome. The concentration of Gd-DTPA-BMA, CBP, PTX of liposome were 106.19 ± 23.53 μg/mg, 2.23 ± 0.37 μg/mg and 9.39 ± 1.71 μg/mg, respectively.

3.2. Lung cancer cell targeting

Three cell lines, including two NSCLC cell lines, A549 and H1299, and a normal cell line, WI-38, were used to test the binding efficiency of the targeted liposome by confocal laser scanning microscopy (CLSM). The RGD peptide has been widely used as a targeting ligand to mediate specific binding to integrin $\alpha_v\beta_3$, which is overexpressed in many cancer cells [8,9,46]. The c(RGDyK)-modified liposome could be internalized via endocytosis mediated by the $\alpha_v\beta_3$ receptor [8,34,36]. RGD-CPGd-L was absorbed more than CPGd-L (Fig. S2) by both cancer cells, indicating the targeting effect of peptide c(RGDyK). As shown in Fig. 3, the red fluorescence intensity of different cells became stronger with increasing incubation time. For NSCLC cells, the fluorescence signals were noticeably strong. The red fluorescence was mainly observed along the cell membranes and within the cytoplasm. The fluorescence intensity of H1299 cells was slightly higher than that of A549 cells, likely resulting from the intrinsic differences between these cell lines, which are known to differ by the density of $\alpha_v\beta_3$ integrin receptors [47]. In contrast, the observed red fluorescence was much weaker in normal cells WI-38, even for incubation times up to 240 min. The results show a remarkably strong contrast for cancers vs normal cells, which we speculate may be related to the vastly different densities of $\alpha_v\beta_3$ receptors at the cell surfaces, for these cell lines [26]. These results suggest that this carrier has the potential to increase drug efficiency and decrease side effects in vivo.

3.3. Drug-mediated cytotoxicity

The anticancer efficiency of RGD-CPGd-L was tested in three different cell lines (cancer cell A549, H1299 and normal cell WI-38) by MTT assay. Different liposomes resulted in dose dependent toxicity on the cells (Fig. 4). The c(RGDyK)-modified liposome can target tumor cells and induce apoptosis [9,35,48]. In two cancer cell lines, cell viability was decreased significantly by treatment with RGD-CPGd-L compared to the non-peptide-modified CPGd-L or single drug-loaded liposome CGd-L or PGd-L (Fig. S3). Cell viability was 48.30% and 55.86% for H1299 and A549, respectively, when RGD-CPGd-L was dosed at concentration up to 12 mg/mL. The targeted liposome was more effective on H1299 than A549 cells, which was in agreement with the fluorescence results. The $\alpha_v\beta_3$ receptor and response of different cancer cells can also vary [7,47]. The blank liposome had a negligible effect on all cell lines. For normal cells, all groups of liposomes had low cytotoxicity, even at high concentrations. Overall, the targeted combination of PTX and CBP demonstrated a synergistic drug effect to tumor cells, which might be superior in cancer treatment.

3.4. In vivo targeted delivery

To evaluate whether such a dual drug-loaded liposome is suitable for in vivo tumor targeting, T_1-weighted MRI was carried out on a 7-T MRI small animal imager before and after administration
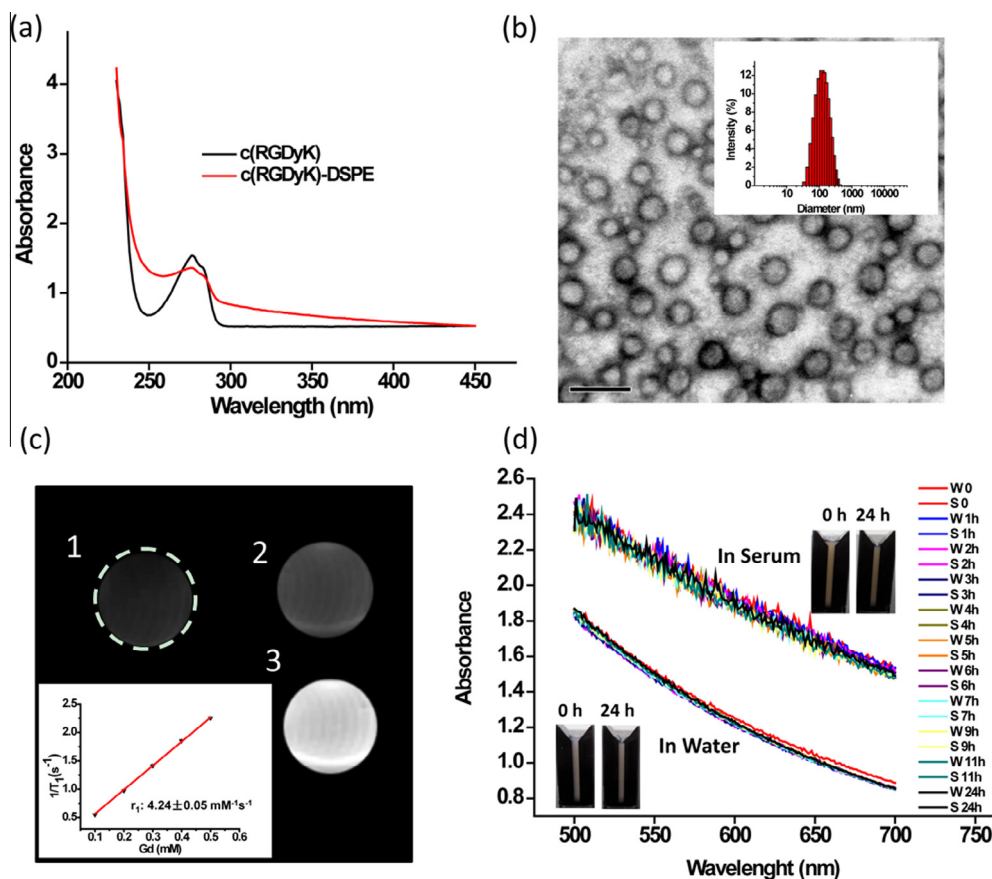
Fig. 2. Characterization of RGD-CPGd-L. (a) UV absorption spectra of the peptide-lipid conjugate c(RGDyK)-PEG2000-DSPE and the peptide c(RGDyK) in methanol/water (4:1, v/v) at the concentration of 1 μM. The absorbance around 270 nm is the benzene of the peptide. (b) Transmission electron micrographs of RGD-CPGd-L with negative staining (scale bar = 200 nm). Insert: DLS measurement of liposome RGD-CPGd-L showing the distribution of diameters and their average size (D = 128 nm). (c) T_1-weighted MR images of phantoms containing 1% agarose (sample 1) and liposome with 0.05 or 0.5 mM Gd-DTPA-BMA (sample 2 and 3). Insert: Spin-lattice $1/T_1$ relaxation rate of RGD-CPGd-L at different concentrations in 98% D_2O with 2% H_2O. The r_1 relaxivity was obtained by comparing the measured (symbols) and theoretical (lines) values. (d) The stability of RGD-CPGd-L (10 mg/mL) in distilled water and serum detected by UV–vis spectrophotometer.

Table 1
Formulation parameters of dual drug-loaded liposome.

Size (nm)	PDI	Zeta potential (mV)
128.4 ± 8.1	0.123	−13.8 ± 4.4
Gd-DTPA-BMA (μg/mg)	CBP (μg/mg)	PTX (μg/mg)
106.19 ± 23.53	2.23 ± 0.37	9.39 ± 1.71

of RGD-CPGd-L via tail vein to A549 xenograft nude mice. For comparison to a non-specific contrast agent, mice were injected with an equal dose of Omniscan®. Fig. 5a clearly demonstrates specific contrast enhancement at the tumor area after administration of the liposome. The tumor of control group also turned bright, but the enhancement was much lower than the case of RGD-CPGd-L. Variations in the spin-lattice relaxation rates R_1 can be seen in Fig. 5b. R_1 was increased more than 10-fold about 4 h and 36-fold nearly 5 h after administration of the new agent compared with the control group. In contrast to the non-treated mouse, R_1 increased about 2.3-fold with the dual drug-loaded liposome. These results demonstrates the targeting effect of the liposome for the tumor site *in vivo*, which is consistent with the results of *in vitro* fluorescence and our MTT assay. Besides solving the problem of PTX insolubility in water and the simultaneous administration of PTX and CBP, this liposome can significantly improve the MRI contrast effect, even at a relatively low dose (100 μmol Gd/kg). The signal enhanced by the targeted liposome maintained a high level for more than 5 h, beginning at 1 h after the treatment,

and returned to original levels after 24 h, indicating good metabolism and giving the investigator substantial time to acquire detailed scans, establish a diagnosis, and conduct and assess the efficacy of drug therapy. In contrast, the MRI signal within the tumor of the control group (Omniscan injection) decreased after 1 h (Fig. S4). PEG coating can form a protective layer over the liposome surface and slow down the recognition by fopsonins, and the subsequent clearance of the particles [30]. This could lead to longer circulation time and a modulation of the EPR (enhanced permeability and retention) effect [20,42]. The enhanced MRI signal and prolonged acting time of contrast agent implies the higher efficiency of delivering small molecules, better performance of tumor inhibition and lower side effects by RGD-CPGd-L than traditional agents.

3.5. Therapeutic effect monitored by MRI

Further, the antitumor efficiency of this dual drug-loaded liposome was studied *in vivo*. First, the body weight of mice was monitored to measure the systemic toxicity of this agent (Fig. 6a). Nearly all mice decreased in weight during the first week, followed by a return of both groups to the initial weight and beyond. This result indicated that there was no detectable systemic toxicity of the liposome. Also there was no acute toxicity observed during and after the experiment.

The antitumor effect was monitored by MRI over a period of 23 days. The volumes of A549 tumors were significantly reduced
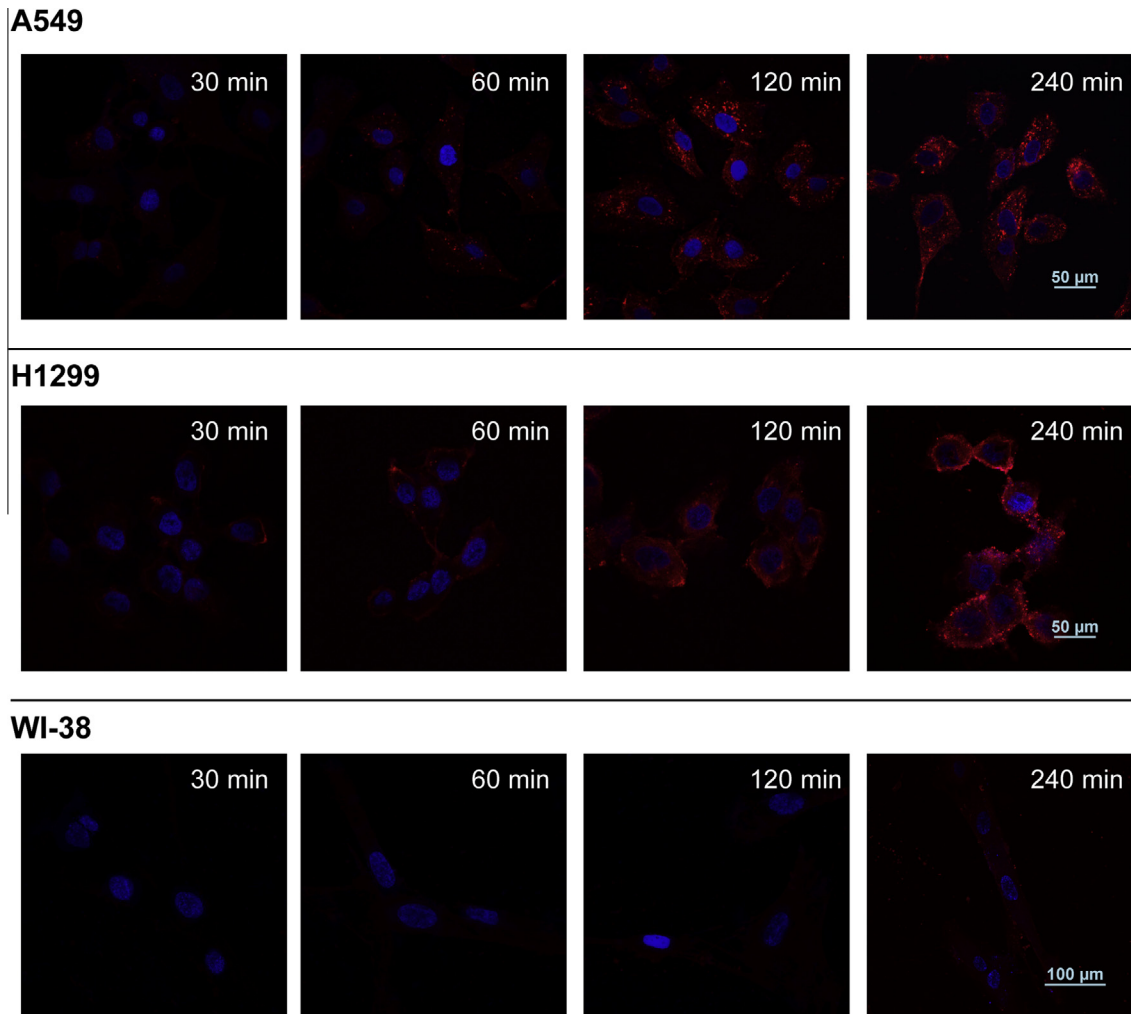
A549

H1299

WI-38

Fig. 3. Fluorescence images of two different lung cancer cells (A549 and H1299) and normal cells (WI-38) incubated with 0.1 mg/mL rhodamine-labeled liposome (Rh-RGD-CPGd-L) at different time. The bright red fluorescence of A549 and H1299 cells indicates the sufficiently endocytosis of Rh-RGD-CPGd-L probes by cancer cells. While negligible fluorescence can be observed in WI-38 cells, indicating favorable selectivity of the designed probe to cancer cells.
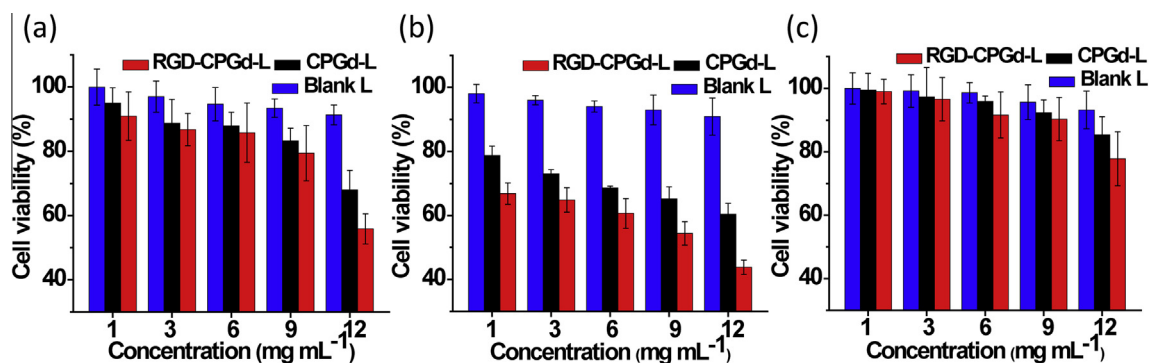

Fig. 4. Liposomal drug efficacies in different cell lines measured by MTT assay. (a), (b) and (c) Cell viabilities of A549, H1299 and WI-38 treated with different groups of liposomes at concentrations of 1, 3, 6, 9 or 12 mg/mL, respectively. The resultant cytotoxicities were determined as percentages of viable cells. Data are presented as mean ± SD, $n \geqslant 3$. RGD-CPGd-L, targeted dual drug-loaded liposome; CPGd-L, dual drug-loaded liposome; blank L, blank liposome. Cell viabilities showed a stronger cytotoxicities of RGD-CPGd-L on cancer cells.

after treatment with dual drug-loaded liposome at day 10 (Fig. 6b). This may be explained by the intense treatment regimen within the first week of therapy. For example, percentage increases of tumor volume were −37.50/−50/−31.25 and 11.11/38.46/50 for liposome group and control group, respectively, at day 10 of the

treatment period. Although the tumors of the liposome group increased in later days, the tumor growth inhibition effect was more obvious than in the control group. The exact tumor variation over time could be clearly seen via T_1-weighted MRIs (Fig. 6c). Mice treated with liposomes had significant tumor growth inhibition
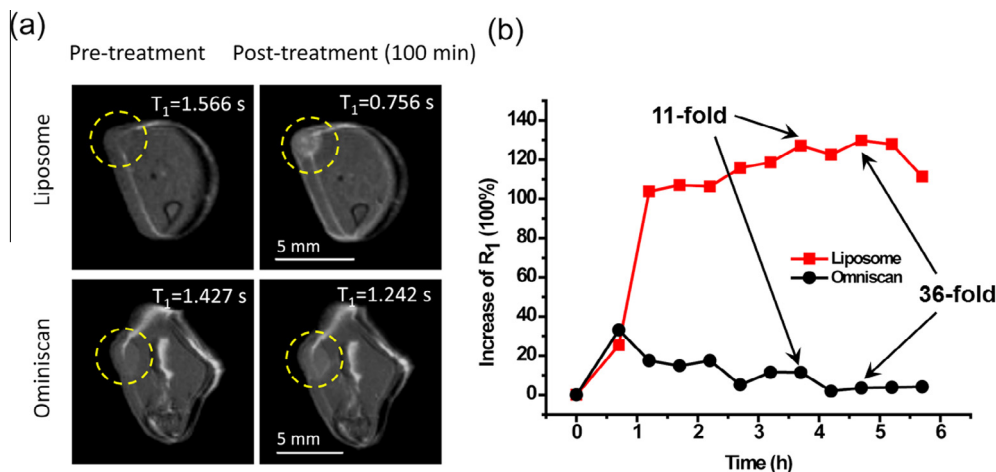
Fig. 5. MRI analysis of the tumors after treatment with RGD-CPGd-L and Omniscan®. (a) T_1-weighted MR images of representative mice before and after the treatment of liposome and omniscan at a concentration of 0.1 mmol Gd/kg. (b) Increase of T_1 relaxation rate (R_1) over time corresponding to the injections. R_1 was enhanced 11-fold 3.7 h and 36-fold 4.7 h after administration of the liposome compared with the commercial MRI contrast agent omniscan.
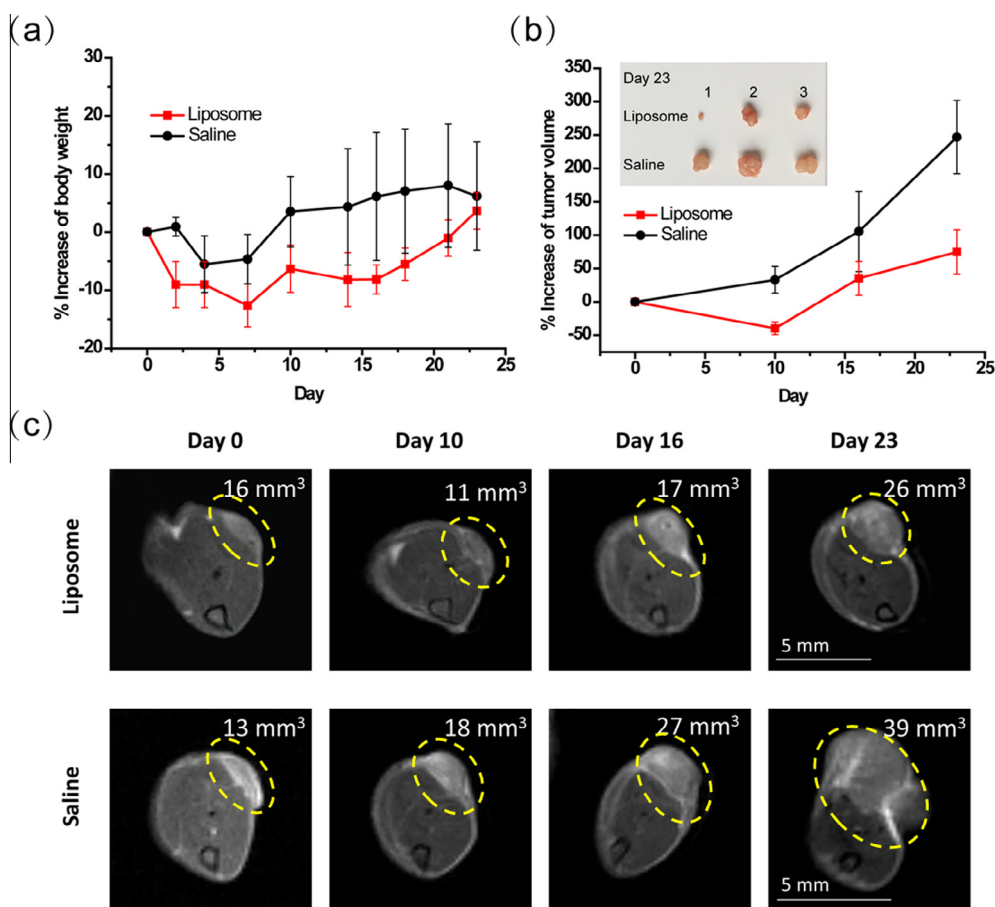

Fig. 6. *In vivo* antitumor efficiency of RGD-CPGd-L on NSCLC cell (A549)-implanted BALB/c mice model assessed by T_1 enhanced MRI. (a) Percentage increase in body weights of mice. Data are presented as mean ± SD, n = 3. (b) Percentage increase of tumor volume as function of time detected by MRI. Data are presented as mean ± SD, n = 3. Insert: photos of the excised tumors after treatment with targeted dual drug-loaded liposome or saline. (c) Representative T_1-weighted MRIs of the tumor on the mice leg at day 0, 10, 16 and 23 after administration of RGD-CPGd-L or RGD-Gd-L. The tumor sizes were 16, 11, 17, 26 mm^3 for targeted dual drug-loaded liposome group, and 13, 18, 27, 39 mm^3 for control group, respectively, at different time points.

compared to the control ones. Particularly, the tumor could be inhibited greatly when the initial volume was small, just as the tumor of the liposome group from 2 mm^3 before treatment to 3 mm^3 at the end of the test (Fig. S5). This is a promising result for early cancer or tumor metastasis control. Moreover, the signal

of the tumor region could be greatly enhanced by this multifunctional liposome even for tumors as small as 1 mm^3 (Fig. S5), demonstrating the efficient targeted delivery of the contrast agent and anti-cancer drugs. Tumor development and therapeutic effect was monitored and evaluated safely and timely by MRI. Further,
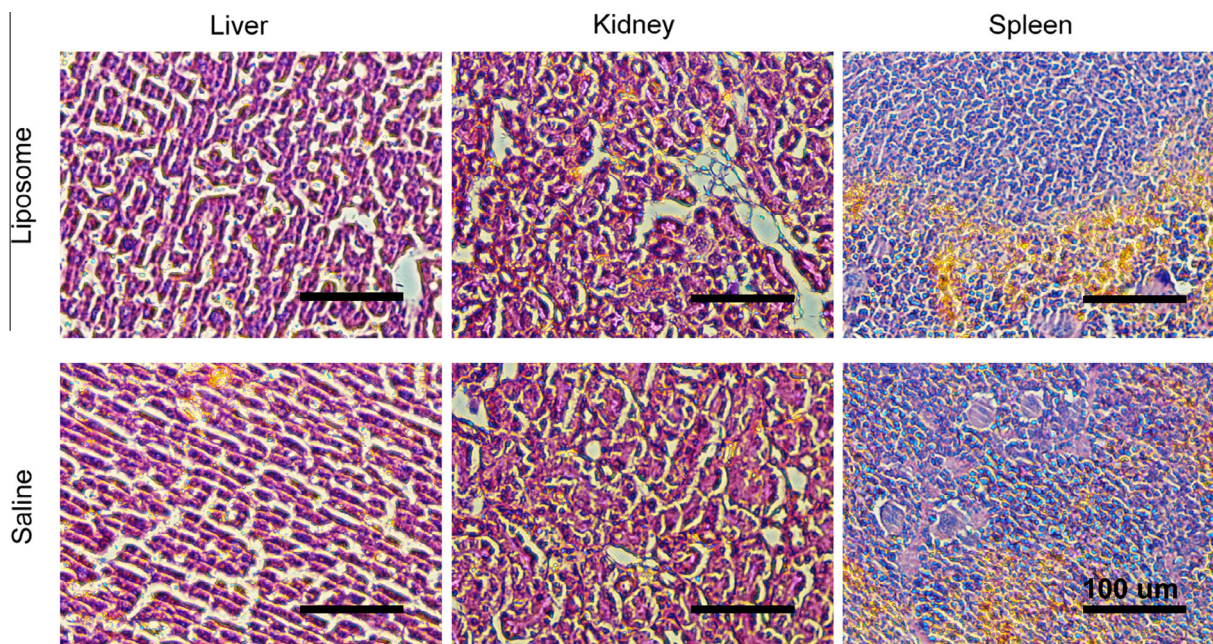
Fig. 7. Representative histopathological results of the mice liver, kidney and spleen 23 days after treatment with liposome and saline.

the development of drug resistance by tumor cells could be impaired when they are treated simultaneously using dual drugs agents rather than a single one [16]. Dual drugs-loaded systems were seldom be developed and mainly on water soluble drugs, just as busulfan/fludarabine [15], irinotecan/floxuridine [16] and irinotecan/cisplatin [17]. Our liposome, contains both hydrophobic paclitaxel and hydrophilic carboplatin, would broaden the scope of drug-loading system. Besides NSCLC, CBP and PTX doublet chemotherapy can also be used in patients with ovarian cancer [49,50]. Based on the researches about liposomal delivery, our system would be an attractive candidate for NSCLC and other cancer treatments.

The histopathological study did not show any distinct changes in the main organs (liver, kidney and spleen) between the treatment and control groups (Fig. 7), indicating this nanoparticle had a negligible toxic effect on the mice. Because of the active tumor targeting, most of the intact liposome might specifically bind to the tumor, thereby decreasing the side effect of the drugs [41]. These results demonstrate that this liposome can be used as a theranostic agent to study the drug behaviors and monitor the therapeutic effects on tumors using MRI.

4. Conclusions

The combination of therapeutic drugs CBP and PTX, together with the diagnostic agent gadodiamide, within a single platform was successfully developed, thereby realizing the simultaneous application of therapeutics and diagnosis. Cytotoxicity tests demonstrated the synergistic effect of this combination. By way of in vitro fluorescence microscopy and *in vivo* MRI, this multifunctional liposome could effectively target non-small-cell lung cancer cells. The tumor signal can be greatly enhanced by employing a Gd-DTPA-BMA-loaded liposome in comparison to the commercial contrast agent Omniscan®. Furthermore, based on the nanoparticles with superior MRI contrast properties, the liposome can provide a non-invasive, real-time MRI strategy with excellent tissue depth penetration and significantly improved sensitivity. Tumor growth could be effectively inhibited with the administration of this drugs-loaded liposome. Consequently, the treatment effects can be evaluated in real-time to allow for optimization of treatment strategies, along the lines of delivering more personalized cancer therapies. Overall, this multifunctional targeted drug delivery system, although needs more studies, constitutes a major advance in the application of nanotechnologies in medicine, opening up new possibilities for the diagnosis and treatment of human diseases.

Appendix A. Supplementary data

Supplementary data associated with this article can be found, in the online version, at http://dx.doi.org/10.1016/j.actbio.2016.02.011.

References

[1] E. Quoix, G. Zalcman, J.P. Oster, V. Westeel, E. Pichon, A. Lavolé, et al., Carboplatin and weekly paclitaxel doublet chemotherapy compared with monotherapy in elderly patients with advanced non-small-cell lung cancer: IFCT-0501 randomized, phase 3 trial, Lancet 378 (2011) 1079–1088.

[2] N. Hanna, F.A. Shepherd, F.V. Fossella, J.R. Pereira, F. Marinis, J. Pawel, et al., Randomized phase III trial of pemetrexed versus docetaxel in patients with non-small-cell lung cancer previously treated with chemotherapy, J. Clin. Oncol. 22 (2004) 1589–1597.

[3] J.H. Schiller, D. Harrington, C.P. Belani, C. Langer, A. Sandler, J. Krook, et al., Comparison of four chemotherapy regimens for advanced non-small-cell lung cancer, New Engl. J. Med. 346 (2002) 92–98.

[4] Y. Ohe, Y. Ohashi, K. Kubota, T. Tamura, K. Nakagawa, S. Negoro, et al., Randomized phase III study of cisplatin plus irinotecan versus carboplatin plus paclitaxel, cisplatin plus gemcitabine, and cisplatin plus vinorelbine for advanced non-small-cell lung cancer: Four-Arm Cooperative Study in Japan, Ann. Oncol. 18 (2007) 317–323.

[5] K. Kelly, J. Crowley, P.A. Bunn, C.A. Presant, P.K. Grevstad, C.M. Moinpour, et al., Randomized phase III trial of paclitaxel plus carboplatin versus vinorelbine plus cisplatin in the treatment of patients with advanced non-small-cell lung cancer: a southwest oncology group trial, J. Clin. Oncol. 19 (2001) 3210–3218.

[6] A. Sandler, R. Gray, M.C. Perry, J. Brahmer, J.H. Schiller, A. Dowlati, et al., Paclitaxel-carboplatin alone or with bevacizumab for non-small-cell lung cancer, New Engl. J. Med. 355 (2006) 2542–2550.

[7] J. Mai, S. Song, M. Rui, D. Liu, Q. Ding, J. Peng, et al., A synthetic peptide mediated active targeting of cisplatin liposomes to Tie2 expressing cells, J. Control. Release 139 (2009) 174–181.

[8] Y. Wang, K. Zhou, G. Huang, C. Hensley, X. Huang, X. Ma, et al., A nanoparticle-based strategy for the imaging of a broad range of tumours by nonlinear amplification of microenvironment signals, Nat. Mater. 13 (2014) 204–212.

[9] X. Ma, J. Jia, R. Cao, X. Wang, H. Fei, Histidine-iridium(III) coordination-based peptide luminogenic cyclization and cyclo-RGD peptides for cancer-cell targeting, J. Am. Chem. Soc. 136 (2014) 17734–17737.

[10] X.H. Peng, Y. Wang, D. Huang, Y. Wang, H.J. Shin, Z. Chen, et al., Targeted delivery of cisplatin to lung cancer using ScFvEGFR-heparin-cisplatin nanoparticles, ACS Nano 5 (2011) 9480–9493.

[11] R.S. Herbst, G. Giaccone, J.H. Schiller, R.B. Natale, V. Miller, C. Manegold, et al., Gefitinib in combination with paclitaxel and carboplatin in advanced non-small-cell lung cancer: a Phase III Trial-INTACT 2, J. Clin. Oncol. 22 (2004) 785–794.

[12] G. Scagliotti, S. Novello, J. Pawel, M. Reck, J.R. Pereira, M. Thomas, et al., Phase III study of carboplatin and paclitaxel alone or with sorafenib in advanced non-small-cell lung cancer, J. Clin. Oncol. 28 (2010) 1835–1842.

[13] P. Saintigny, Recent advances in non-small cell lung cancer biology and clinical management, Discov. Med. 13 (2012) 287–297.

[14] M.W. Ndinguri, R. Solipuram, R.P. Gambrell, S. Aggarwal, R.P. Hammer, Peptide targeting of platinum anti-cancer drugs, Bioconjugate Chem. 20 (2009) 1869–1878.

[15] U. Gergis, G. Roboz, T. Shore, E. Ritchie, S. Mayer, U. Wissa, et al., A phase I study of CPX-351 in combination with busulfan and fludarabine conditioning and allogeneic stem cell transplantation in adult patients with refractory acute leukemia, Biol. Blood Marrow Tr. 19 (2013) 1040–1045.

[16] P.G. Tardi, R.C. Gallagher, S. Johnstone, N. Harasym, M. Webb, M.B. Bally, et al., Coencapsulation of irinotecan and floxuridine into low cholesterol-containing liposomes that coordinate drug release in vivo, BBA-Biomembranes 1768 (2007) 678–687.

[17] P.G. Tardi, N.D. Santos, T.O. Harasym, S.A. Johnstone, N. Zisman, A.W. Tsang, et al., Drug ratio-dependent antitumor activity of irinotecan and cisplatin combinations in vitro and in vivo, Mol. Cancer Ther. 8 (2009) 2266–2275.

[18] L. Ren, S. Chen, H. Li, Z. Zhang, C. Ye, M. Liu, et al., MRI-visible liposome nanovehicles for potential tumor-targeted delivery of multimodal therapies, Nanoscale 7 (2015) 12843–12850.

[19] N.V. Koshkina, J.C. Waldrep, L.E. Roberts, E. Golunski, S. Melton, V. Knight, Paclitaxel liposome aerosol treatment induces inhibition of pulmonary metastases in murine renal carcinoma model, Clin. Cancer Res. 7 (2001) 3258–3262.

[20] S. Koudelka, J. Turánek, Liposomal paclitaxel formulations, J. Control. Release 163 (2012) 322–334.

[21] P. Crosasso, M. Ceruti, P. Brusa, S. Arpicco, F. Dosio, L. Cattel, Preparation, characterization and properties of sterically stabilized paclitaxel-containing liposomes, J. Control. Release 63 (2000) 19–30.

[22] P. Ma, R.J. Mumper, Paclitaxel nano-delivery systems: a comprehensive review, J. Nanomed. Nanotechnol. 4 (2013) 1–16.

[23] V.P. Torchilin, Recent advances with liposomes as pharmaceutical carriers, Nat. Rev. Drug Discov. 4 (2005) 145–160.

[24] B. Baruah, A. Surin, Interaction of liposome-encapsulated cisplatin with biomolecules, J. Biol. Inorg. Chem. 17 (2012) 899–910.

[25] G.P. Stathopoulos, D. Antoniou, J. Dimitroulis, P. Michalopoulou, A. Bastas, K. Marosis, et al., Liposomal cisplatin combined with paclitaxel versus cisplatin and paclitaxel in non-small-cell lung cancer: a randomized phase III multicenter trial, Ann. Oncol. 21 (2010) 2227–2232.

[26] C.M. Lee, T. Tanaka, T. Murai, M. Kondo, J. Kimura, W. Su, et al., Novel chondroitin sulfate-binding cationic liposomes loaded with cisplatin efficiently suppress the local growth and liver metastasis of tumor cells in vivo, Cancer Res. 62 (2002) 4282–4288.

[27] X. Wang, J. Zhou, Y. Wang, Z. Zhu, Y. Lu, Y. Wei, et al., A phase I clinical and pharmacokinetic study of paclitaxel liposome infused in non-small cell lung cancer patients with malignant pleural effusions, Eur. J. Cancer 46 (2010) 1474–1480.

[28] A. Chaudhury, S. Das, R.M. Bunte, G.N.C. Chiu, Potent therapeutic activity of folate receptor-targeted liposomal carboplatin in the localized treatment of intraperitoneally grown human ovarian tumor xenograft, Int. J. Nanomed. 7 (2012) 739–751.

[29] S. Biswas, N.S. Dodwadkar, P.P. Deshpande, V.P. Torchilin, Liposomes loaded with paclitaxel and modified with novel triphenylphosphonium-PEG-PE conjugate possess low toxicity, target mitochondria and demonstrate

[30] enhanced antitumor effects in vitro and in vivo, J. Control. Release 159 (2012) 393–402.

[30] Y. Liu, N. Zhang, Gadolinium loaded nanoparticles in theranostic magnetic resonance imaging, Biomaterials 33 (2012) 5363–5375.

[31] T. Tagami, W.D. Foltz, M.J. Ernsting, C.M. Lee, I.F. Tannock, J.P. May, et al., MRI monitoring of intratumoral drug delivery and prediction of the therapeutic effect with a multifunctional thermosensitive liposome, Biomaterials 32 (2011) 6570–6578.

[32] K. Na, S.A. Lee, S.H. Jung, B.C. Shin, Gadolinium-based cancer therapeutic liposomes for chemotherapeutics and diagnostics, Colloid. Surface. B. 84 (2011) 82–87.

[33] E. Cittadino, M. Ferraretto, E. Torres, A. Maiocchi, B.J. Crielaard, T. Lammers, et al., MRI evaluation of the antitumor activity of paramagnetic liposomes loaded with prednisolone phosphate, Eur. J. Pharm. Sci. 45 (2012) 436–441.

[34] Y. Miura, T. Takenaka, K. Toh, S. Wu, H. Nishihara, M.R. Kano, et al., Cyclic RGD-linked polymeric micelles for targeted delivery of platinum anticancer drugs to glioblastoma through the blood–brain tumor barrier, ACS Nano 7 (2013) 8583–8592.

[35] G.K. Seward, Y. Bai, N.S. Khan, I.J. Dmochowski, Cell-compatible, integrin-targeted cryptophane-129Xe NMR biosensors, Chem. Sci. 2 (2011) 1103–1110.

[36] S. Xu, B.Z. Olenyuk, C.T. Okamoto, S.F.H. Alvarez, Targeting receptor-mediated endocytotic pathways with nanoparticles: rationale and advances, Adv. Drug Deliver. Rev. 65 (2013) 121–138.

[37] Y. Katanasaka, T. Ishii, T. Asai, H. Naitou, N. Maeda, F. Koizumi, et al., Cancer antineovascular therapy with liposome drug delivery systems targeted to BiP/GRP78, Int. J. Cancer 127 (2010) 2685–2698.

[38] J. Du, W.L. Lu, X. Ying, Y. Liu, P. Du, W. Tian, et al., Dual-targeting topotecan liposomes modified with tamoxifen and wheat germ agglutinin significantly improve drug transport across the blood–brain barrier and survival of brain tumor-bearing animals, Mol. Pharm. 6 (2009) 905–917.

[39] Y. Liu, W.L. Lu, J. Guo, J. Du, T. Li, J.W. Wu, et al., A potential target associated with both cancer and cancer stem cells: a combination therapy for eradication of breast cancer using vinorelbine stealthy liposomes plus parthenolide stealthy liposomes, J. Control. Release 129 (2008) 18–25.

[40] Y. Yoshizawa, K. Ogawara, A. Fushimi, S. Abe, K. Ishikawa, T. Araki, et al., Deeper penetration into tumor tissues and enhanced in vivo antitumor activity of liposomal paclitaxel by pretreatment with angiogenesis inhibitor SU5416, Mol. Pharm. 9 (2012) 3486–3494.

[41] V.P. Chekhonin, V.P. Baklaushev, G.M. Yusubalieva, A.E. Belorusova, M.V. Gulyaevd, E.B. Tsitrinc, et al., Targeted delivery of liposomal nanocontainers to the peritumoral zone of glioma by means of monoclonal antibodies against GFAP and the extracellular loop of Cx43, Nanomed. Nanotechnol. 8 (2012) 63–70.

[42] S. Kaida, H. Cabral, M. Kumagai, A. Kishimura, Y. Terada, M. Sekino, et al., Visible drug delivery by supramolecular nanocarriers directing to single-platformed diagnosis and therapy of pancreatic tumor model, Cancer Res. 70 (2010) 7031–7041.

[43] M. Hossann, T. Wang, Z. Syunyaeva, M. Wiggenhorn, A. Zengerle, R.D. Issels, et al., Non-ionic Gd-based MRI contrast agents are optimal for encapsulation into phosphatidyldiglycerol-based thermosensitive liposomes, J. Control. Release 166 (2013) 22–29.

[44] G. Mikhaylov, U. Mikac, A.A. Magaeva, V.I. Itin, E.P. Naiden, I. Psakhye, et al., Ferri-liposomes as an MRI-visible drug-delivery system for targeting tumours and their microenvironment, Nat. Nanotechnol. 6 (2011) 594–602.

[45] S. Meng, B. Su, W. Li, Y. Ding, L. Tang, W. Zhou, et al., Enhanced antitumor effect of novel dual-targeted paclitaxel liposomes, Nanotechnology 21 (2010) 1–7.

[46] P.P. Shah, M.Y. Fong, S.S. Kakar, PTTG induces EMT through integrin AlphaV Beta3-focal adhesion kinase signaling in lung cancer cells, Oncogene 31 (2012) 3124–3135.

[47] R. Yao, A. Sui, Z. Wang, S. Liu, Q. Zhou, X. Liu, et al., Induction of non-small cell lung carcinoma apoptosis using soluble RGD-TRAIL by targeting the integrin receptor of tumor cells, Mol. Med. Rep. 6 (2012) 1355–1360.

[48] J.S. Desgrosellier, D.A. Cheresh, Integrins in cancer: biological implications and therapeutic opportunities, Nat. Rev. Cancer 10 (2010) 9–22.

[49] R.F. Ozols, B.N. Bundy, B.E. Greer, J.M. Fowler, D.C. Pearson, R.A. Burger, et al., Phase III trial of carboplatin and paclitaxel compared with cisplatin and paclitaxel in patients with optimally resected stage III ovarian cancer: a gynecologic oncology group study, J. Clin. Oncol. 21 (2003) 3194–3200.

[50] P.A. Vasey, G.C. Jayson, A. Gordon, H. Gabra, R. Coleman, R. Atkinson, et al., Phase III randomized trial of docetaxel-carboplatin versus paclitaxel-carboplatin as first-line chemotherapy for ovarian carcinoma, J. Natl. Cancer I. 96 (2004) 1682–1691.